

# **Intercellular contact is sufficient to drive fibroblast-to-myofibroblast transitions**

Vasuretha Chandar<sup>1</sup>, Benjamin M. Goykadosh<sup>1</sup> & Harikrishnan Parameswaran<sup>1\*</sup>

<sup>1</sup>Department of Bioengineering, Northeastern University, Boston, MA, USA

\*Harikrishnan Parameswaran, Ph.D. (corresponding author)

## **Abstract**

Fibroblast cells play a key role in maintaining the extracellular matrix. During wound healing, fibroblasts differentiate into highly contractile myofibroblasts, which secrete extracellular matrix proteins like collagen to facilitate tissue repair. Under normal conditions, myofibroblasts undergo programmed cell death after healing to prevent excessive scar formation. However, in diseases like fibrosis, the myofibroblasts remain active even after the wound is closed, resulting in excessive collagen buildup and a stiff, fibrotic matrix. The reasons for the persistence of myofibroblasts in fibrosis are not well understood. Here, we show the existence of a mechanism where direct physical contact between a fibroblast and a myofibroblast is sufficient for fibroblasts to transition into myofibroblasts. We demonstrate that the fibroblast-myofibroblast transition can occur even in the absence of known biochemical cues, such as growth factor activation or mechanical cues from a stiff, fibrotic matrix. Furthermore, we demonstrate that contact-based fibroblast-myofibroblast activation can be inhibited by the Gαq/11/14 inhibitor FR900359, which prevents the formation of myofibroblasts. These findings provide new insights into the persistence of fibrosis despite therapeutic interventions, suggesting a potential strategy for targeting the fibroblast-to-myofibroblast transition in fibrotic conditions.

## **Significance Statement**

This study uncovers a novel mechanism of fibroblast-to-myofibroblast transition (FMT) in fibrosis, challenging traditional views. This study demonstrates that direct fibroblast-myofibroblast contact

can drive FMT independently of biochemical signals and matrix stiffness. The GqGPCR signaling pathway is identified as a key mediator of this process, offering a new therapeutic target. Additionally, increased cytoskeletal tension in fibroblasts is found to precede and drive FMT, suggesting mechano-therapeutic potential. By highlighting the role of cell-cell interactions and mechanical forces in fibrosis, this research fills a critical knowledge gap and opens new avenues for treatment.

## **Introduction**

Idiopathic Pulmonary Fibrosis (IPF) is a chronic, progressive interstitial lung disease of unknown etiology<sup>1,2</sup>. Despite the lack of a clear cause, several risk factors have been identified, including aging and air pollution, which can trigger injury to lung tissues<sup>3,4</sup>. At the site of injury, one of the key cellular processes is the transformation of resident fibroblasts into highly contractile myofibroblasts<sup>5</sup>. These specialized cells, characterized by  $\alpha$ -smooth muscle actin ( $\alpha$ -SMA) expression, play a crucial role in wound contraction and tissue remodeling at the site of injury by depositing extracellular matrix components, particularly collagen, to facilitate tissue repair<sup>6-12</sup>. In normal wound healing, once tissue integrity is restored, myofibroblasts are typically deactivated and cleared from the site<sup>13,14</sup>. However, in IPF, this process becomes dysregulated, leading to the persistent activation and accumulation of myofibroblasts<sup>14,15</sup>. This results in excessive collagen deposition, causing scarring, stiffening, and fibrosis of the lung tissue. The stiffening of the lung severely impairs the ability of the lungs to facilitate oxygen and carbon dioxide exchange, leading to organ dysfunction - contributing to the progressive nature of the disease, leading to hypoxemia, loss of quality of life, and ultimately death<sup>16,17</sup>. As such, the persistence of the myofibroblast phenotype plays a crucial role in the progression of IPF.

Current therapeutic strategies aim to prevent or reverse myofibroblast activation through two main approaches. The first involves targeting growth factors such as the WNT/ $\beta$ -catenin, PDGF, and TNF- $\alpha$ , among others<sup>18</sup>. Existing drugs (ex: Nintedanib, Pirfenidone) inhibit growth factors and cytokines, which prevent the release of inflammatory signals that trigger the transition of fibroblasts to myofibroblasts<sup>19,20</sup>. The second approach recognizes the mechanosensitive nature of fibroblasts and focuses on matrix remodeling. Fibroblasts can sense the stiff fibrotic environment created by excessive collagen deposition and transform into myofibroblasts that secrete more collagen reinforcing a detrimental feedback loop<sup>21-23</sup>. To counteract this cycle, ongoing in vitro and in vivo studies are investigating matrix remodeling as a potential therapeutic approach<sup>24-26</sup>. These studies utilize collagen-degrading enzymes, such as matrix metalloproteinases (MMPs), to soften the matrix and potentially halt the disease progression of the phenotype<sup>27-29</sup>. However, despite these interventions, IPF continues to progress, suggesting that additional mechanisms are at play that remain unknown. The goal of this study is to identify alternative mechanisms responsible for the persistence of myofibroblasts in fibrotic conditions.

## **Results**

### **1. Fibroblasts can transition into myofibroblasts even in the absence of biochemical signals or mechanical cues from a stiff extracellular matrix.**

To test whether fibroblasts can transition to myofibroblasts without external chemical or mechanical cues, we generated two distinct cell populations: a fibroblast population that does not express  $\alpha$ -SMA in stress fibers was generated by culture on a 300Pa soft substrate for 6 weeks. Similarly, a myofibroblast population expressing  $\alpha$ -SMA in stress fibers was generated by culturing fibroblasts on tissue culture plastic ( $E \geq 100$ kPa), for 4 weeks. To identify fibroblasts in a co-culture

with myofibroblasts, we labeled fibroblasts with a fluorescent td-tomato reporter (magenta). Myofibroblasts that express the reporter indicate the fibroblast that transitioned into a myofibroblast in culture. The cells were then seeded to maintain a 1:1 ratio of fibroblasts to myofibroblasts ( $10^5$  cells/cm<sup>2</sup>) on a 300Pa (soft substrate) for 72 hours under standard cell culture conditions. No external mechanical signals (Stiff substrate) or chemical stimuli (e.g., TGF $\beta$ ) were introduced to facilitate phenotype transitions. After 72 hours, the fibroblast cells were stained for filamentous actin (F-actin) and alpha-smooth muscle actin ( $\alpha$ -SMA) in the stress fibers. To assess their phenotypic characteristics, we also measured the nuclear spread area of fibroblasts and myofibroblasts<sup>30</sup>. We counted the number of transformed fibroblasts in a given field of view (40X) and found that  $20 \pm 5$  fibroblasts in the co-culture expressed  $\alpha$ SMA in their stress fibers as compared to fibroblasts in mono-culture (**Fig. 1A-C**,  $p=0.008$ , t-test,  $N=3$ ). Further, there was no difference in the nuclear spread area of the fibroblasts when co-cultured with myofibroblasts, confirming a phenotypic transition of fibroblasts into myofibroblasts (**Fig. 1D-E**, One-way ANOVA,  $N=3$ ). Notably, this transition occurs in the absence of external chemical or mechanical stimuli, suggesting that cell-cell interactions within the co-culture environment may be responsible for driving this phenotypic change.

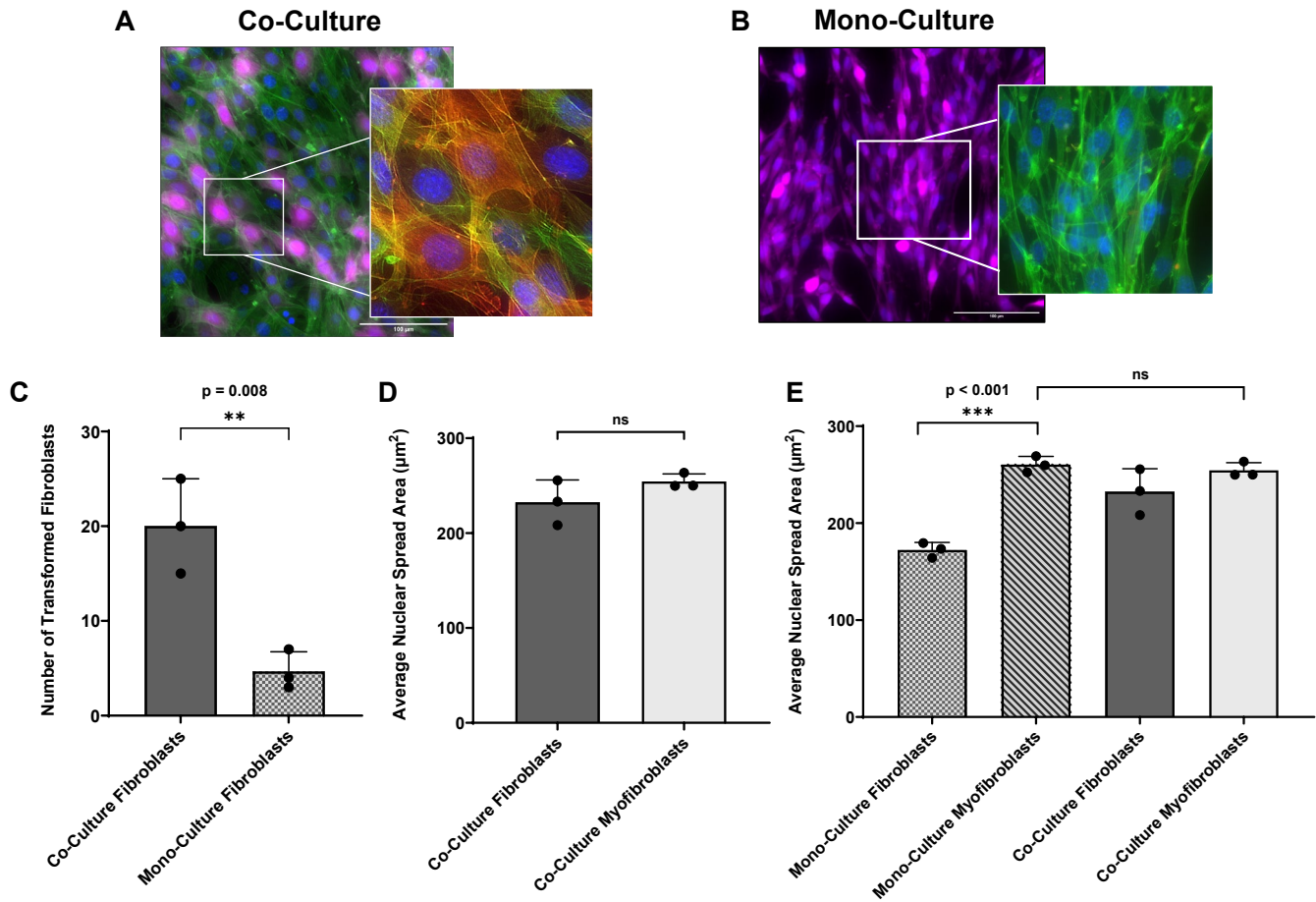


**Fig 1: Fibroblasts when co-cultured with myofibroblasts on a soft ( $E=300\text{Pa}$ ) PDMS substrate, undergo a phenotypic shift to myofibroblasts despite the absence of external biochemical stimuli (like growth factors) or mechanical stimuli from stiff substrate.** Cells were stained for myofibroblast markers f-actin (green) and  $\alpha$ -SMA (red) and nuclear stain DAPI (blue) after 3 days in culture. **(A)** Fibroblasts (magenta) in co-culture with myofibroblasts showed sequestration of  $\alpha$ -SMA in their stress fibers when cultured on a 300Pa soft substrate, as in the inset (indicated by reddish-yellow stress fibers). **(B)** Fibroblasts in monoculture on 300Pa soft substrate retained their phenotype when not in contact with myofibroblasts. Scale bars 100 $\mu\text{m}$ . **(C)** A significant number of fibroblasts ( $20 \pm 5$  cells) transformed into myofibroblasts as compared to fibroblasts in monoculture ( $4.66 \pm 2.08$ ) ( $p = 0.008$ , unpaired t-test,  $n=3$ ). **(D)** There is no significant difference in the nuclear spread area of fibroblasts in a co-culture compared to myofibroblasts in the co-culture (unpaired t-test,  $n=3$ ). **(E)** There is no significant difference in the nuclear spread area of

fibroblasts and myofibroblasts in the co-culture when compared to that of myofibroblasts in a monoculture (One-way ANOVA, n=3).

## **2. Intercellular contact facilitates fibroblast-to-myofibroblast transition (FMT)**

To better understand the mechanism underlying the transition of fibroblasts to myofibroblasts, even in the absence of external cues, we hypothesized that fibroblasts and myofibroblasts communicate with each other to facilitate FMT transitions. To test this hypothesis and identify the primary mechanism for FMT transitions in coculture, we used a 3D-printed barrier (~1.5mm thick) to split our culture dishes into two halves. (**Fig. 2A**) On one side of the barrier, we cultured myofibroblasts, and on the other side, we cultured fibroblasts. We maintained the 1:1 ratio of fibroblasts & myofibroblasts (as in **Fig. 1**). On both sides of the barrier, cells were cultured on soft (E=300Pa) nusil gels. The barrier prevented contact between fibroblasts and the myofibroblasts. However, the barrier allowed the diffusion of chemical signals, as evidenced by the immediate diffusion of red dye across both sides of the barrier (**Fig. 2B**). Cells were cultured under standard cell culture conditions for 72 hours. The cells were stained for f-actin and  $\alpha$ SMA in the stress fibers to determine whether fibroblasts transformed into myofibroblasts. Cells that underwent FMT were identified by the presence of TD tomato reporter and alpha-smooth muscle actin in the stress fibers (**Fig. 2C**). We counted the number of fibroblasts that underwent FMT within a field of view, averaged over N=3 independent trials. With the barrier in place preventing direct physical contact, only a statistically insignificant number of fibroblasts ( $1.3 \pm 0.57$  cells,  $p < 0.001$ , t-test) showed signs of alpha-smooth muscle actin in stress fibers. However, after removing the barrier,  $20 \pm 2$  fibroblasts transitioned into myofibroblasts (**Fig. 2D**). These findings indicate that cell-to-cell contact between a fibroblast and a myofibroblast is sufficient for the fibroblast-to-myofibroblast transition.

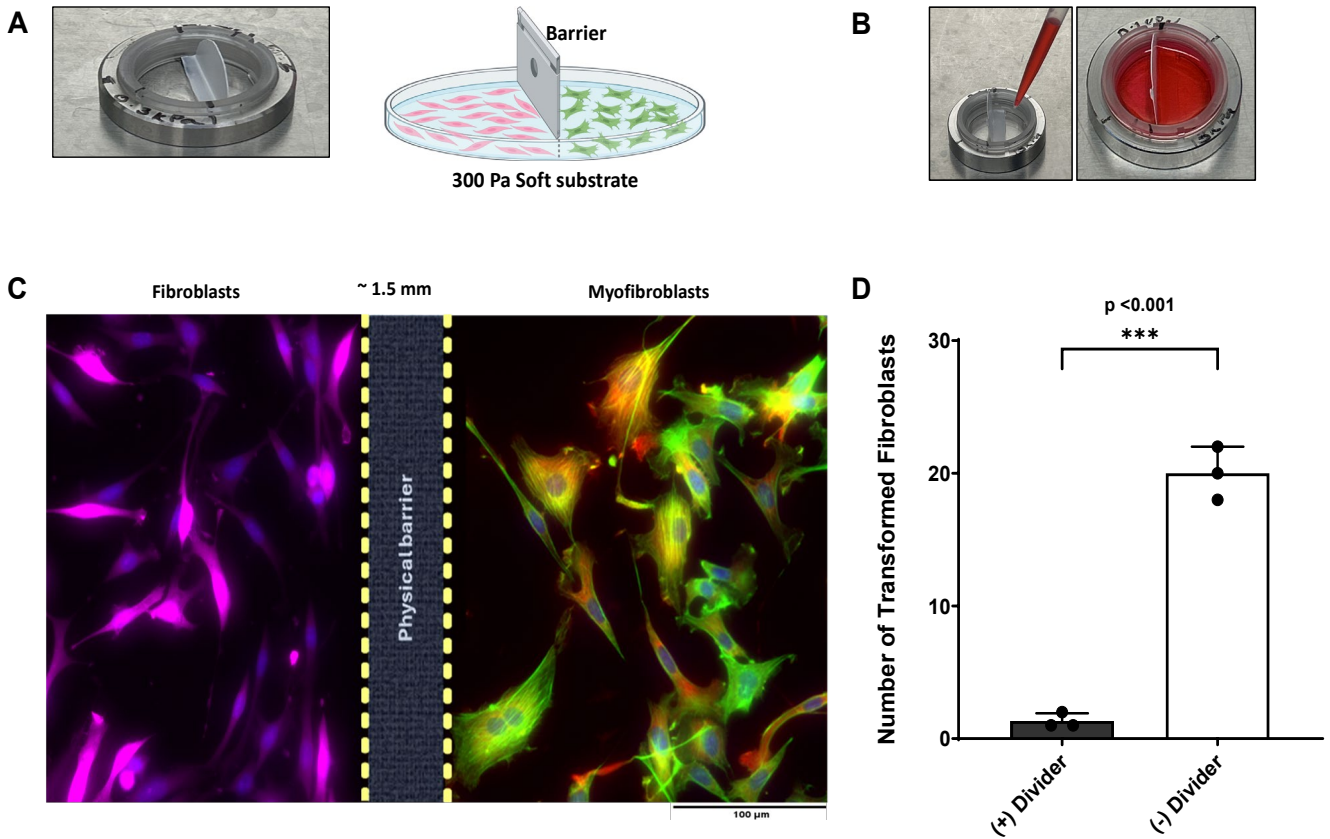


**Fig 2: Cell-cell contact is sufficient for fibroblast-to-myfibroblast transitions. (A)** A physical barrier set up on the 300Pa soft substrate separates fibroblasts from the myfibroblasts. The drawing shows fibroblasts in pink and myfibroblasts in green on either side of the divider. **(B)** The immediate diffusion of red dye across the dish in the presence of the barrier confirmed the possibility of diffusion of any intercellular chemical signals. **(C)** Cells were stained for myofibroblast markers, F-actin (green) and  $\alpha$ -SMA (red), and nuclear stain DAPI (blue). Fibroblasts (magenta) did not express  $\alpha$ -SMA in their stress fibers when not in contact with myofibroblasts despite the presence of intercellular chemical signals, but myofibroblasts retained their phenotype (visible reddish-yellow stress fibers). Scale bar 100 $\mu$ m. **(D)** With the divider in place, only  $1.3 \pm 0.57$  fibroblasts showed signs of alpha-smooth muscle actin in stress fibers and in the absence of divider,  $20 \pm 2$  fibroblasts transitioned into myfibroblasts ( $p < 0.001$ , unpaired t-test,  $n=3$ ).

### **3. Contact between fibroblasts and myofibroblasts results in an increase of cytoskeletal tension in fibroblasts**

As a next step, we investigated the potential role of mechanosensitive signaling in the cell-contact-dependent transition of fibroblasts to myofibroblasts. Prior research has demonstrated that fibroblasts exhibit lower intrinsic cytoskeletal tension (cellular pre-stress) compared to myofibroblasts<sup>24,31</sup>. We hypothesized that upon contact with myofibroblasts, the high cytoskeletal tension in myofibroblasts may alter the cytoskeletal tension in fibroblasts, thereby triggering the fibroblast-to-myofibroblast transition. In our study, we used a publicly available implementation of Monolayer Stress Microscopy (MSM) to quantify the mechanical stresses within the cells in the co-culture and calculate the net cellular contractility ( $M_{ii}$ )<sup>32,33</sup>. The MSM technique combines Traction Force Microscopy (TFM) with computational modeling to generate stress maps, allowing us to visualize and measure the internal mechanical tension across the cell monolayer<sup>34-36</sup>. Briefly, the fibroblasts and myofibroblasts were co-cultured into a multicellular photopatterned ensemble. Cells were imaged after 24 hours of seeding, and we measured the traction forces exerted by cells onto a deformable  $E=13\text{kPa}$  substrate embedded with fluorescent beads. By applying a mask that outlines cell-cell borders from a phase-contrast image, we reconstructed the force vectors at the cell-substrate interface. Using these traction forces as input, MSM enabled us to compute the in-plane stresses within the monolayer, providing a detailed map of mechanical tensions between cells where we were able to separately calculate contractility due to cell-cell interactions, cell-matrix interactions, and the net contractility of each cell, as well as determine the normal and shear forces at each cell border by analyzing bead displacements<sup>32</sup>. The underlying assumptions and limitations of this method have been detailed in previous work<sup>33</sup>.



We observed that fibroblasts in direct contact with myofibroblasts in the co-culture exhibited increased cytoskeletal tension ( $M_{ii}$ ), showing no statistical difference between myofibroblast and the first neighbor fibroblasts on day 1 (**Fig. 3C**, Mann-Whitney Rank Sum Test,  $p=0.004$ ,  $N=2$ ). This data is particularly of interest because no visible phenotypic changes are detected in the fibroblasts after 24 hours of co-culture with myofibroblasts on 300Pa soft substrate. Specifically, we do not observe the expression of  $\alpha$ SMA in stress fibers (**Fig. 3D**) and the nuclear spread area of fibroblasts is significantly lower than that of myofibroblasts (**Fig. 3E**, One-way ANOVA,  $p=0.034$ ,  $N=3$ ). The findings from this work are the first to suggest that an increase in cytoskeletal tension precedes phenotypic transition from fibroblasts to myofibroblasts, providing insight into the mechanical aspects of this cellular transformation.

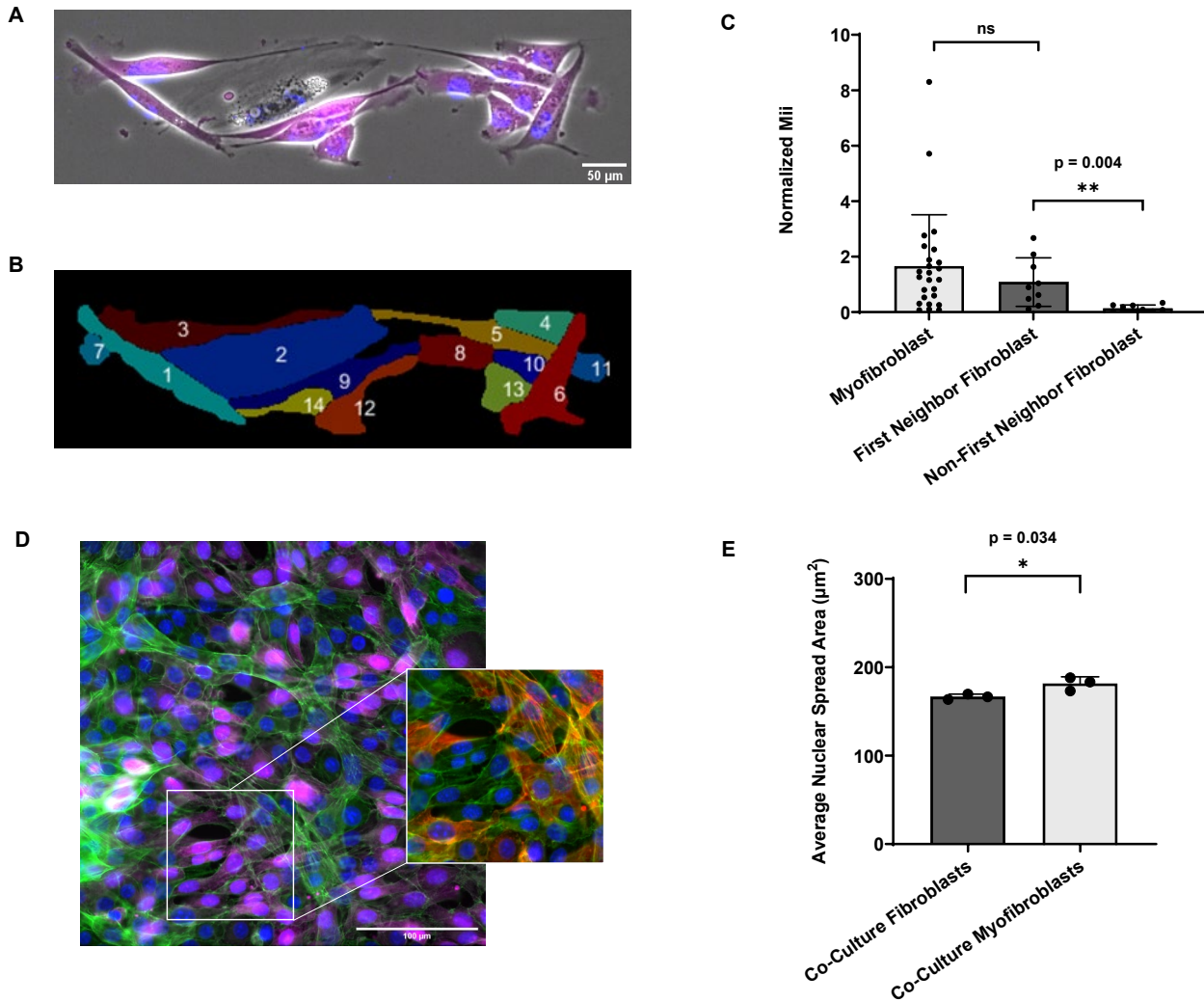


**Fig 3: Fibroblasts in contact with myofibroblasts exhibit increased cytoskeletal tension in 24 hours (1 day of contact with myofibroblasts).** (A-B) representative pattern of a cellular ensemble of a myofibroblast-fibroblast culture. Nuclei are stained blue, with fibroblasts-stained (magenta). Here, cell 2 is a myofibroblast, with 1, 3, 9 and 5 considered “first neighbor fibroblast” as they are in direct contact with the myofibroblast, and the remaining cells are “non-first neighbor fibroblasts” as they are not in direct contact with myofibroblasts. Scale bar 50 $\mu\text{m}$ . (C) Fibroblasts in contact with a myofibroblast exhibit increased contractility ( $M_{ij}$ ) within 24 hours, reaching levels comparable to myofibroblasts, indicating an early mechanical transition before a documented phenotypic change (Mann-Whitney Rank Sum Test,  $n=2$ ). In contrast, fibroblasts without direct myofibroblast contact show significantly lower contractility ( $p = 0.004$ ,

Mann-Whitney Rank Sum Test, n=2). **(D)** Fibroblasts do not express  $\alpha$ -SMA in their stress fibers, indicating that they do not transition into myofibroblasts despite being in contact with myofibroblasts for 24 hours (indicated by the absence of reddish-yellow stress fibers). Scale bar 100 $\mu$ m. **(E)** The average nuclear spread area of fibroblasts in the co-culture, is significantly lower than that of the myofibroblasts in the same culture, indicating a lack of phenotype transition (One-way ANOVA, p=0.034, n=3).

#### **4. An increase in cytoskeletal tension is sufficient to drive the fibroblast-to-myofibroblast transition**

To determine if an increase in cell prestress alone is sufficient to drive fibroblast-to-myofibroblast transition (FMT), fibroblast monocultures on the 300 Pa substrate were treated with 2.5 $\mu$ M histamine, a compound known to increase cytoskeletal prestress but not directly influence fibroblast to myofibroblast transition<sup>37</sup>. Our observations from N=3 independent trials reveal that  $16.6 \pm 4.5$  fibroblasts in the fibroblast mono-culture transitioned into myofibroblasts as compared to untreated controls, suggesting that an increase in cytoskeletal prestress alone can induce fibroblast to myofibroblast transition (**Fig. 4A-D**, t-test, p=0.015, N=3). The temporal relationship between the increase in cytoskeletal tension and the subsequent phenotypic transition suggests a causal link between these two phenomena. These findings not only shed light on the mechanical aspects of the fibroblast-to-myofibroblast transformation but also underscore the importance of cell-cell interactions and mechanical forces in regulating cellular behavior and FMT. This contributes to our understanding of the complex interplay between cellular mechanics and phenotypic plasticity in the context of tissue remodeling and fibrosis.

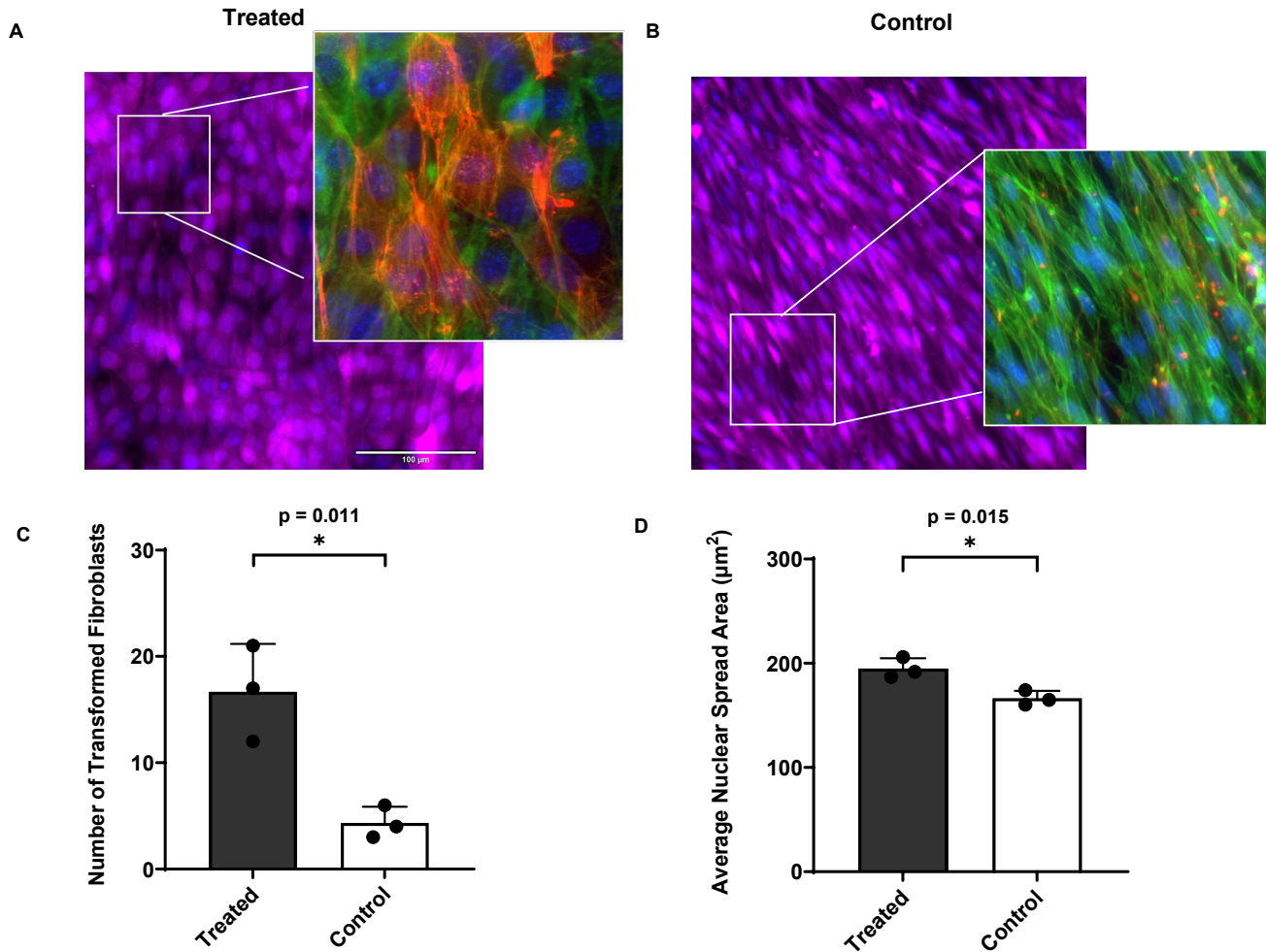


**Fig 4: A rise in cytoskeletal pre-stress is sufficient to induce the transition of fibroblasts to myofibroblasts even in the absence of myofibroblast contact on a 300Pa soft substrate. (A)** Fibroblasts (magenta) that are treated with 2.5μM histamine (72 hours) to increase their cytoskeletal pre-stress, show sequestration of α-SMA in their stress fibers (indicated by reddish yellow stress fibers). **(B)** Fibroblasts (controls not treated with Histamine) do not show α-SMA in their stress fibers (indicated by the absence of reddish yellow stress fibers). Scale bars 100μm. **(C)** A significant number of fibroblasts ( $16.6 \pm 4.5$  cells) transformed into myofibroblasts in response to increased cellular pre-stress alone when on a 300Pa soft substrate, compared to the controls,  $4.3 \pm 1.5$  cells (unpaired t-test,  $p=0.011$ ,  $n=3$ ). **(D)** The average nuclear

spread area of fibroblasts is significantly higher than the control, indicating a phenotype transition due to a rise in cellular pre-stress (unpaired t-test,  $p=0.015$ ,  $n=3$ ).

## **5. Mechanical activation of Gq GPCR pathways is essential for contact-based FMT**

It is well-established that signal transduction across cell membranes involves the activation of two key enzymes: phosphatidylinositol (PI)-specific phospholipase C (PLC) and phosphoinositide 3-kinase (PI 3-kinase)<sup>38</sup>. Typically, PLC activation occurs in response to various cellular agonists. In our study, we hypothesized that cells in contact utilize mechanical force as a stimulus to initiate PLC activation (**Fig. 5A**). Specifically, we hypothesized that a shear stress of 20Pa is sufficient to trigger PLC activation. Myofibroblast can exert shear stress of the order of 1 kPa<sup>39</sup>. The shear stress that we apply here is a small fraction of the stress exerted by a myofibroblast. This shear generates force to activate Phospholipase C, triggering the hydrolysis of Phosphatidylinositol 4,5-bisphosphate (PI(4,5)P<sub>2</sub> or PIP<sub>2</sub>). The hydrolysis results in the production of two important second messengers: inositol 1,4,5-trisphosphate (I(1,4,5)P<sub>3</sub> or IP<sub>3</sub>) and diacylglycerol (DAG)<sup>38,40,41</sup>.

To test the existence of a force-induced PLC activation mechanism in fibroblasts, we used an indenter to apply a shear stress of 20Pa calculated based on displacements of beads attached to the gel, and the stiffness of the gel. We observed a systematic decline in PIP<sub>2</sub> levels (measured as fluorescence intensity) in the cell ensemble, confirming PLC activation and PIP<sub>2</sub> hydrolysis (**Fig. 5B**). To test whether mechanical activation of G $\alpha$ q pathways was involved in contact-based FMT transitions, we used FR900359, a cyclic depsipeptide inhibitor of G $\alpha$ q, G $\alpha$ 11, and G $\alpha$ 14 in a co-culture of fibroblasts and myofibroblasts on soft ( $E=300\text{Pa}$ ) substrate<sup>42</sup>. Cells were grown under standard culture conditions and treated with 10 $\mu\text{M}$  FR900359 for 72 hours (controls were samples that did not receive treatment). Staining for myofibroblast markers revealed that when the co-culture was treated with 10 $\mu\text{M}$  FR900359 only  $2.33\pm 0.57$  fibroblasts transitioned into

myofibroblasts in the presence of the GqGPCR inhibitor despite being in contact with myofibroblasts as compared to untreated controls (**Fig. 5D-E**,  $p < 0.001$ , unpaired t-test,  $N=3$ ). Myofibroblasts remained unaffected under both conditions. These findings provide valuable insight into the molecular mechanism underlying fibroblast to myofibroblast transitions, suggesting that the GqGPCR pathway is triggered upon myofibroblast contact with fibroblast and inhibition of this pathway prevents cell-cell contact-induced transition.

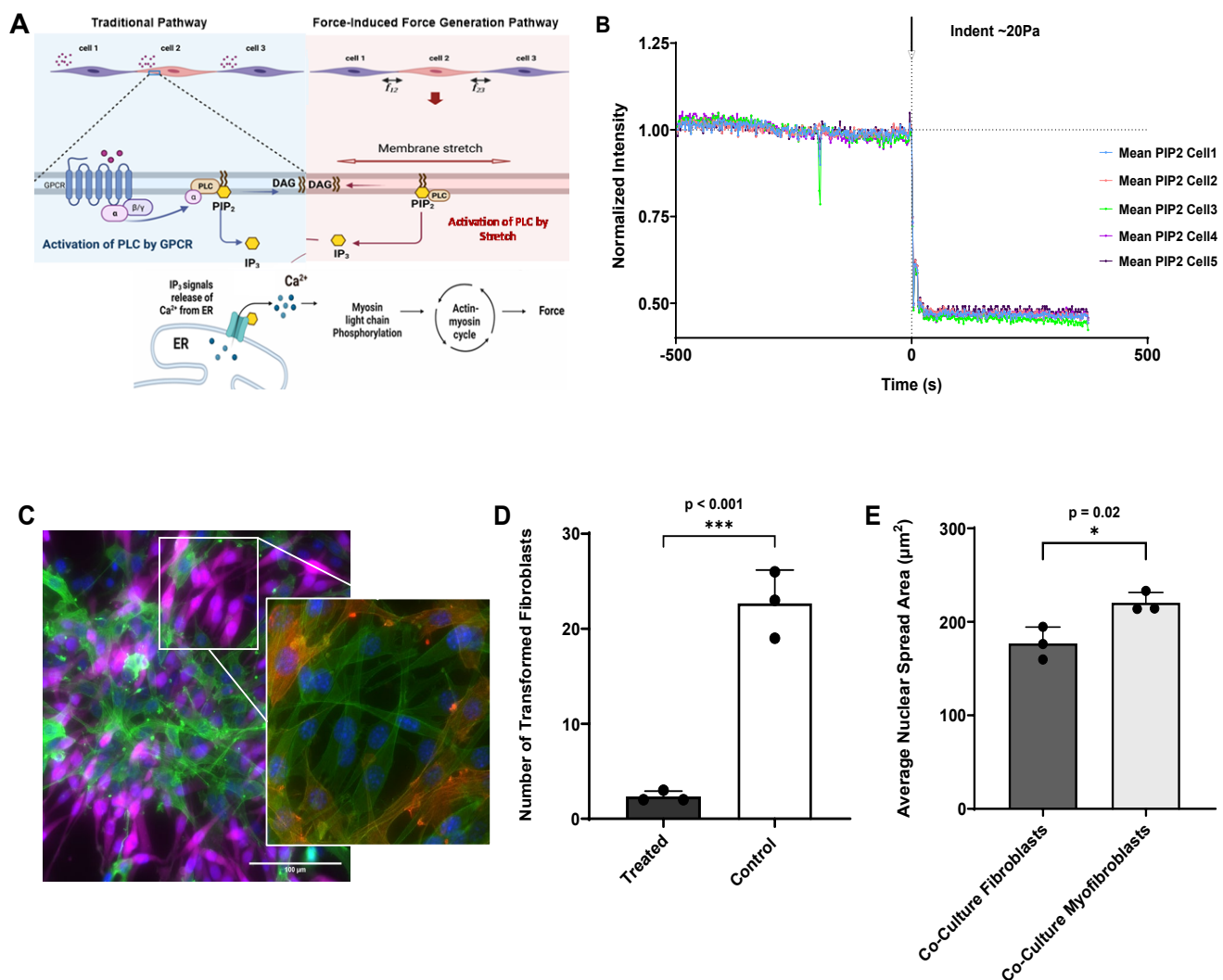


**Fig 5: Cell-cell contact induces PIP2 hydrolysis and blocking the GqGPCR pathway prevents cell-cell contact induced fibroblast to myofibroblast transitions on a 300Pa soft substrate. (A)** The diagram shows a force-induced force-generation mechanism in fibroblasts. Here cells in contact utilize mechanical force as a stimulus to initiate PLC activation, just as an agonist would in the traditional pathway. **(B)** A shear stress of ~20 Pa was sufficient to induce PLC activation and result in PIP2 hydrolysis, indicated by a steady decline in PIP2 fluorescence intensity (n=1). When cells were stained for myofibroblast markers, F-actin (green) and  $\alpha$ -SMA (red) and nuclear stain DAPI (blue) **(C)** Fibroblasts do not show  $\alpha$ -SMA in their stress fibers, indicating that they do not transition into myofibroblasts in the presence of the GqGPCR inhibitor despite being in a co-culture for 3 days. Scale bar 100 $\mu$ m. **(D)** Only a negligible fraction of fibroblasts ( $2.33 \pm 0.57$  cells) transitioned to myofibroblasts in the presence of the inhibitor ( $p < 0.001$ , unpaired t-test, n=3). **(E)** The average nuclear spread area of fibroblasts in the co-culture when GqGPCR pathway is inhibited, is significantly lower than that of the myofibroblasts in the same culture, indicating a lack of phenotype transition (One-way ANOVA, n=3).

## **Discussion**

This study uncovers novel mechanisms driving fibroblast-to-myofibroblast transition (FMT) in fibrosis, challenging the traditional view that FMT is primarily governed by soluble factors or extracellular matrix (ECM) stiffness. We demonstrate that direct cell-cell contact between fibroblasts and myofibroblasts is sufficient to induce FMT, independent of biochemical or matrix-derived mechanical cues. Our findings emphasize the critical role of intercellular mechanical signaling and highlight the GqGPCR pathway as a mediator of contact-induced FMT, presenting a promising target for anti-fibrotic therapies. Furthermore, the observed increase in cytoskeletal tension preceding and driving FMT suggests that modulating cellular mechanics could be an effective therapeutic strategy. While these results provide significant insights, limitations remain. The in vitro nature of the experiments may not fully capture the complexity of in vivo fibrotic

environments. Future studies should validate these findings in 3D culture systems or animal models and further dissect the molecular mechanisms linking cell-cell contact, GqGPCR signaling, and cytoskeletal tension to FMT. Identifying key mechanotransduction players could uncover additional therapeutic targets. Further investigation into the role of specific mechanosensitive proteins and ion channels could provide additional insights into the mechanotransduction pathways involved in fibroblast-to-myofibroblast transition. Exploring the interplay between cellular mechanics and epigenetic regulation during this process may reveal novel mechanisms of fibrosis progression. Additionally, developing targeted approaches to modulate cytoskeletal tension in specific cell populations within fibrotic tissues could lead to more precise and effective therapeutic interventions.

In conclusion, this study reveals a previously unrecognized mechanism of FMT driven by direct cell-cell interactions and mechanical signaling, expanding our understanding of fibrosis progression. By highlighting the interplay between intercellular mechanical forces and cytoskeletal tension, this work opens new avenues for therapeutic interventions targeting the mechanical aspects of fibrotic disease.

## **Materials and Methods**

1. **Fabrication of an optically clear substrate:** NuSil is an optically clear, biologically inert PDMS substrate with a tunable Young's modulus ranging from 0.3 to 70 kPa. To model soft healthy tissue, equal parts of NuSil gel-8100, parts A and B (NuSil, CA, USA) were mixed (1:1) to obtain a substrate with Young's modulus  $E=300\text{Pa}$  and spin-coated onto 30-mm-diameter, #1.5 glass coverslips for 50 seconds to produce a  $100\mu\text{m}$ -thick layer. Similarly, a crosslinker volume 0.36% of the combined parts A and B volume was added to obtain substrates with Young's modulus  $E = 13\text{ kPa}$ . Coverslips were incubated at room temperature for an hour and cured overnight at



60°C. These cured coverslips were then secured in sterile 40-mm Bioptech dishes (Biological Optical Technologies, PA, USA), UV sterilized for 1 hour, and protein coated with 0.1% gelatin solution (Millipore Sigma) for use in cell culture experiments.

2. **Fibroblast Culture:** NIH 3T3 mouse fibroblasts (Lot #70030679) acquired from ATCC were utilized for our experiments. Cells were grown under standard culture conditions of 37°C and 5% CO<sub>2</sub> and used by passage 20 for all experiments. Culture medium: Cells were cultured in 10% fetal bovine serum, Dulbecco's modified Eagle's medium/F12 (Fisher Scientific, Massachusetts), 1× penicillin/streptomycin (Fisher Scientific), 1× MEM nonessential amino acid solution (Sigma Aldrich, Missouri), and amphotericin B (25 µg/liter; Sigma-Aldrich). Co-culture platform to study fibroblast-to-myofibroblast transition: Equal number of fibroblasts and myofibroblasts (1:1) were plated together (or with a physical barrier to separate the cell types while allowing diffusion) on the 300Pa soft substrate. At a seeding density of 10<sup>5</sup> cells per cm<sup>2</sup>, the cells were cultured in standard cell culture medium and conditions as above, for 72 hours in the absence of any external chemical (eg: TGFβ<sub>1</sub>)/ stiff matrix mechanical cues. Cells were then analyzed for fibroblast to myofibroblast transitions.
3. **Generation of a fibroblast and myofibroblast population:** To visualize and distinctively identify fibroblasts, NIH 3T3-mouse fibroblasts (ATCC) were transduced with a lentiviral vector encoding tandem-dimer Tomato fluorescence protein (tdTomato, Vector Builder, catalog no. VB181014-1005thm). Briefly, the cells were seeded and cultured according to standard cell culture protocol and after 18 hours, cells were introduced to cell culture medium containing polybrene (5 µg/ml; Thermo Fisher Scientific, catalog no. TR1003G) and the manufacturer's recommended functional titer concentration of lentiviruses. After 24 hours of exposure to the transduction medium, cells were allowed to recover in unadulterated cell culture medium for

an additional 48 hours. Next, cells were harvested using Gibco TrypLE Select reagent and cell selection was performed by culturing cells on 300Pa soft substrate in culture medium containing blasticidin (8 µg/ml; Sigma-Aldrich, catalog no. 15205). This 3T3-mouse fibroblast population expressing tdTomato (3T3-tdT) was expanded on protein coated 300Pa soft substrates and cultured for up to at least 6 weeks before being used in experiments, or they were continued to be expanded on the soft substrate for use within 20 passages since the time of thawing. To generate a myofibroblast population, non-transduced 3T3-mouse fibroblasts were cultured for a period of at least 4 weeks on tissue culture plastic ( $\geq 100$ kPa) and utilized within passage 20 for all experiments. Myofibroblasts were identified as cells that stained positive for  $\alpha$ -SMA in stress fibers.

4. **Immunostaining and microscopy:** Cells were fluorescently labeled for filamentous actin (F-actin) and alpha smooth muscle actin ( $\alpha$ -SMA). Cells were fixed in 4% paraformaldehyde in PBS at room temperature for 10 minutes. Then, cells were permeabilized with 100% ethanol for 10 min at 20°C. Following permeabilization, cells were blocked using 1× PBS containing 0.1% Tween 20, 1% bovine serum albumin (BSA), and glycine (22.52 mg/ml) for 30 min at room temperature. Next, cells were labelled with Alpha-Smooth Muscle Actin Monoclonal Antibody (1A4), eFluor™ 660, eBioscience™ (Cat #50-9760-82) at 5 µg/mL in 1× PBS containing 1% BSA and simultaneously stained for Filamentous actin with ActinGreen™ 488 ReadyProbes™ Reagent (AlexaFluor™ 488 phalloidin, Cat# R37110) for 1 hour at room temperature. Cells were washed 3 times with 1X PBS to remove non-specific binding. Lastly, cell nuclei were labeled with NucBlue (Fisher Scientific, Waltham, MA, USA) and mounted using ProLong™ Glass Antifade Mountant (Cat #P36984). Images were acquired with a Leica DMI8 inverted microscope, a Leica

DFC6000 camera, and a Leica LED8 light engine (excitation, 480/40 nm; emission, 527/50 nm) using a 40x/0.65 dry objective (Leica DMI8 microscope, Leica, Wetzlar, Germany).

5. **Applying a point displacement on the matrix:** We fixed a nail dotting tool (ORLY, California) with a 1.5 mm diameter ball-end to the InjectMan 4 micromanipulator (Eppendorf, Germany) on our Leica DMI8 microscope. The micromanipulator allowed precise control of this tool with which we applied a transient poke to the extracellular matrix some distance away ( $\sim 300\mu\text{m}$ ) from adhered cells at a  $45^\circ$  angle and depth of  $30\mu\text{m}$  to generate a shear stress of the order of 10s of Pa, comparable to that of a myofibroblast.
6. **Fluorescent PIP2 Imaging:** Fibroblasts were loaded with a fluorescent cytosolic PIP2 indicator to record changes in [PIP2] using a live green downward phosphatidylinositol 4,5-biphosphate (PIP2) assay kit (#D0400G), Montana Molecular (Montana). The assay genetically encodes fluorescent protein expression using a BacMam vector. Following the protocol provided, we transduced cultured fibroblasts with the PIP2 sensor for 24 hours at  $37^\circ\text{C}$  and 5%  $\text{CO}_2$ . Prior to imaging, cells were washed with Hanks' Balanced Salt Solution (HBSS) and incubated at  $37^\circ\text{C}$  and 5%  $\text{CO}_2$  in for an additional 30 minutes. The cells were washed once more before imaging. 16-bit images were recorded at 0.5 Hz for 5 minutes before indentation ( $\sim 20\text{Pa}$ ) and at least 5 minutes post indentation. Cells were imaged with a Leica DMI8 inverted microscope, a Leica DFC6000 camera, and a Leica LED8 light engine (excitation, 480/40 nm; emission, 527/50 nm) with a 40x/0.65 dry objective. The excitation and emission wavelengths for the PIP2 was ex:480 nm/ em:515 nm. To analyze data, each image sequence was loaded in Fiji ImageJ, and regions of interest (ROIs) were hand-selected in the cytoplasm of each cell to obtain mean grayscale intensities over the area of the ROI for each frame in time. Obtained intensities were normalized with the baseline average to plot normalized intensity values using GraphPad Prism ver. 10.4.1.

7. **Patterning cell ensembles:** We utilized the Alvéole's PRIMO optical module and the Leonardo software, a UV-based, contactless photopatterning system (Alvéole, Paris, France). 13kPa NuSil substrates coated with a layer of fluorescent beads as fiducial markers for traction force microscopy were utilized. A 5% solution of 0.2- $\mu\text{m}$ -diameter green, fluorescent carboxylate-modified microspheres (FluoSpheres, Invitrogen, Carlsbad, CA, USA) in PBS was vortexed for 10 seconds. Solution (2 ml) was added to each substrate in a Biotech dish and left at room temperature for 1 hour to allow the beads to adhere. The bead solution was poured off, substrates were washed three times with PBS, and then PBS was poured off. Substrates were then protein coated with 0.1% gelatin solution for use in cell culture. The substrate surface was first coated with 500  $\mu\text{g}/\text{mL}$  PLL (Sigma Aldrich, St. Louis, MO, USA) for 1 hour at room temperature. The substrate was washed with PBS and 10 mM HEPES buffer adjusted to pH 8.0 and incubated with 50  $\text{mg}/\text{mL}$  mPEG-SVA (Laysan Bio, Inc., Arab, AL, USA) at room temperature for 1 hour, and washed with PBS once more. The PRIMO system was calibrated using fluorescent highlighter on an identical substrate. The PBS was replaced by 14.5  $\text{mg}/\text{mL}$  PLPP (Alvéole, Paris, France), and then the desired pattern, previously created with graphic software, was illuminated with UV light focused on the substrate surface for 30 seconds. Patterned surfaces were washed again with PBS and then incubated with 0.1% gelatin for 1 hour at room temperature. The substrate was washed and hydrated in standard cell culture media. Fibroblasts and myofibroblasts were added in a 1:1 ratio totaling a cell density of  $3 \times 10^4$  cells/ml to obtain a confluent pattern of the two cell types within 24 hours.
8. **Traction Force Microscopy and Monolayer Stress Microscopy measurements:** Traction forces were recorded by imaging the fluorescent beads with a 20x/0.55 dry objective and the Leica DMI8 microscope. Images were taken at baseline, during the experiment, and after cells were

removed (using RLT Lysis Buffer, Qiagen, Hilden, Germany). Using these images, cellular forces were calculated with a custom MATLAB (MathWorks, Natick, MA, USA) software program using Fourier Traction Force Microscopy (TFM). To calculate the net contractility of each cell within a multicellular ensemble, we employed monolayer stress microscopy (MSM). This computational approach estimates stresses in a cell layer based on the forces at the cell-matrix interface. Initially, traction force vectors obtained from traction force microscopy (TFM) were processed using a modified version of the open-source Python code, pyTFM. By applying a mask that outlines cell-cell borders from a phase-contrast image, we were able to separately calculate contractility due to cell-cell interactions, cell-matrix interactions, and the net contractility of each cell, as well as determine the normal and shear forces at each cell border.

9. **Measurement of nuclear spread area:** The nuclear spread area represented in this manuscript is the average nuclear area of 10 cells in each dish (n). 40X images were loaded into Fiji ImageJ, and regions of interest (ROIs) were hand-selected in the DAPI images using the ellipse tool, by tracing the outline of the nucleus. The area of selection was spatially calibrated using the Analyze>Set Scale option and calculated in square pixels and represented as  $\mu\text{m}^2$ .
10. **Data presentation and statistical testing:** Throughout the manuscript, we represent data as the average of N independent trials. The error bars indicate SD over independent trials. The individual data points are shown in all bar plots. SigmaPlot ver.11 build 11.0.0.75 (Systat Software, San Jose, CA) was used to perform statistical tests. One-way ANOVAs followed by post-hoc pairwise comparisons were used to test for significant differences in datasets of three or more groups, which were influenced by one independent factor. Pairwise comparisons were performed using the t-test when data were normally distributed. Otherwise, the Mann-Whitney rank-sum test was used to compare median values. Statistical significance was reported using

asterisks, where  $p < 0.05$  (\*),  $p < 0.01$  (\*\*),  $p < 0.001$  (\*\*\*). The specific tests used, number of samples, and p values are described along with the corresponding results.

### **Acknowledgements**

The authors thank Ms. Christina Velez for providing the EFS-tdTomato lentivirus. This work was supported by the National Science Foundation (NSF) Career grant #2047207 awarded to Harikrishnan Parameswaran.

**Author Contributions:** H.P. conceived the research and developed the overall hypothesis, and V.C. and H.P. designed the experiments. V.C. conducted the experiments, analyzed the experimental data, and interpreted the results, along with V.C. and HP. V.C. prepared the figures. B.M.G. and V.C. performed the monolayer stress traction microscopy, B.M.G. analyzed the monolayer stress traction microscopy data, prepared the figures, and interpreted the results of both the monolayer stress traction microscopy and traction force microscopy experiments. V.C., B.M.G., and H.P. contributed to the drafting, editing, and revision of the manuscript. H.P. approved the final version of the manuscript.

**Competing Interest Statement:** None of the authors have any competing interests to declare.

**Classification:** Major classification: Physical Sciences>Engineering

**Minor classification:** Biological Sciences >Biophysics

### **References**

1. Spagnolo, P. *et al.* Idiopathic pulmonary fibrosis: Disease mechanisms and drug development. *Pharmacol Ther* **222**, 107798 (2021).
2. Martinez, F. J. *et al.* Idiopathic pulmonary fibrosis. *Nat Rev Dis Primers* **3**, 17074 (2017).

3. Raghu, G., Weycker, D., Edelsberg, J., Bradford, W. Z. & Oster, G. Incidence and Prevalence of Idiopathic Pulmonary Fibrosis. *Am J Respir Crit Care Med* **174**, 810–816 (2006).
4. Johannson, K. A. *et al.* Acute exacerbation of idiopathic pulmonary fibrosis associated with air pollution exposure. *European Respiratory Journal* **43**, 1124–1131 (2014).
5. Hinz, B. Formation and Function of the Myofibroblast during Tissue Repair. *Journal of Investigative Dermatology* **127**, 526–537 (2007).
6. Darby, I., Skalli, O. & Gabbiani, G. Alpha-smooth muscle actin is transiently expressed by myofibroblasts during experimental wound healing. *Lab Invest* **63**, 21–9 (1990).
7. Desmouliere, A., Darby, I. A., Laverdet, B. & Bonté, F. Fibroblasts and myofibroblasts in wound healing. *Clin Cosmet Investig Dermatol* 301 (2014) doi:10.2147/CCID.S50046.
8. Serini, G. & Gabbiani, G. Mechanisms of Myofibroblast Activity and Phenotypic Modulation. *Exp Cell Res* **250**, 273–283 (1999).
9. Hinz, B., Celetta, G., Tomasek, J. J., Gabbiani, G. & Chaponnier, C. Alpha-Smooth Muscle Actin Expression Upregulates Fibroblast Contractile Activity. *Mol Biol Cell* **12**, 2730–2741 (2001).
10. Wang, J., Zohar, R. & McCulloch, C. A. Multiple roles of  $\alpha$ -smooth muscle actin in mechanotransduction. *Exp Cell Res* **312**, 205–214 (2006).
11. Hinz, B., Celetta, G., Tomasek, J. J., Gabbiani, G. & Chaponnier, C. *Alpha-Smooth Muscle Actin Expression Upregulates Fibroblast Contractile Activity. Molecular Biology of the Cell* vol. 12 (2001).
12. Hinz, B., Dugina, V., Ballestrem, C., Wehrle-Haller, B. & Chaponnier, C. A-Smooth Muscle Actin Is Crucial for Focal Adhesion Maturation in Myofibroblasts. *Molecular Biology of the Cell* vol. 14 2508–2519 Preprint at <https://doi.org/10.1091/mbc.E02-11-0729> (2003).
13. Hinz, B. The role of myofibroblasts in wound healing. *Curr Res Transl Med* **64**, 171–177 (2016).
14. Ju, X. *et al.* Regulation of myofibroblast dedifferentiation in pulmonary fibrosis. *Respir Res* **25**, 284 (2024).
15. Moore, M. W. & Herzog, E. L. Regulation and Relevance of Myofibroblast Responses in Idiopathic Pulmonary Fibrosis. *Curr Pathobiol Rep* **1**, 199–208 (2013).
16. Plantier, L. *et al.* Physiology of the lung in idiopathic pulmonary fibrosis. *European Respiratory Review* **27**, 170062 (2018).

17. Burgess, J. K. & Harmsen, M. C. Chronic lung diseases: entangled in extracellular matrix. *European Respiratory Review* **31**, 210202 (2022).
18. Plikus, M. V. *et al.* Fibroblasts: Origins, definitions, and functions in health and disease. *Cell* **184**, 3852–3872 (2021).
19. Noble, P. W. *et al.* Pirfenidone in patients with idiopathic pulmonary fibrosis (CAPACITY): two randomised trials. *Lancet* **377**, 1760–9 (2011).
20. Wollin, L. *et al.* Mode of action of nintedanib in the treatment of idiopathic pulmonary fibrosis. *Eur Respir J* **45**, 1434–45 (2015).
21. Wells, R. G. The role of matrix stiffness in regulating cell behavior. *Hepatology* **47**, 1394–1400 (2008).
22. Elson, E. L., Qian, H., Fee, J. A. & Wakatsuki, T. A model for positive feedback control of the transformation of fibroblasts to myofibroblasts. *Prog Biophys Mol Biol* **144**, 30–40 (2019).
23. Hong, Y. *et al.* Cell–matrix feedback controls stretch-induced cellular memory and fibroblast activation. *Proceedings of the National Academy of Sciences* **122**, (2025).
24. Tomasek, J. J., Gabbiani, G., Hinz, B., Chaponnier, C. & Brown, R. A. Myofibroblasts and mechano: Regulation of connective tissue remodelling. *Nature Reviews Molecular Cell Biology* vol. 3 349–363 Preprint at <https://doi.org/10.1038/nrm809> (2002).
25. Tschumperlin, D. J., Ligresti, G., Hilscher, M. B. & Shah, V. H. Mechanosensing and fibrosis. *J Clin Invest* **128**, 74–84 (2018).
26. Freeberg, M. A. T. *et al.* Mechanical Feed-Forward Loops Contribute to Idiopathic Pulmonary Fibrosis. *Am J Pathol* **191**, 18–25 (2021).
27. Staab-Weijnitz, C. A. Fighting the Fiber: Targeting Collagen in Lung Fibrosis. *Am J Respir Cell Mol Biol* **66**, 363–381 (2022).
28. Craig, V. J., Zhang, L., Hagood, J. S. & Owen, C. A. Matrix metalloproteinases as therapeutic targets for idiopathic pulmonary fibrosis. *Am J Respir Cell Mol Biol* **53**, 585–600 (2015).
29. Henry, M. T. *et al.* Matrix metalloproteinases and tissue inhibitor of metalloproteinase-1 in sarcoidosis and IPF. *Eur Respir J* **20**, 1220–7 (2002).
30. Hillsley, A. *et al.* A strategy to quantify myofibroblast activation on a continuous spectrum. *Sci Rep* **12**, 12239 (2022).



31. Li, B. & Wang, J. H.-C. Fibroblasts and myofibroblasts in wound healing: force generation and measurement. *J Tissue Viability* **20**, 108–20 (2011).
32. Bauer, A. *et al.* pyTFM: A tool for traction force and monolayer stress microscopy. *PLoS Comput Biol* **17**, e1008364 (2021).
33. Tambe, D. T. *et al.* Monolayer Stress Microscopy: Limitations, Artifacts, and Accuracy of Recovered Intercellular Stresses. *PLoS One* **8**, e55172 (2013).
34. Tambe, D. T. *et al.* Collective cell guidance by cooperative intercellular forces. *Nat Mater* **10**, 469–475 (2011).
35. Patel, N. G. *et al.* Unleashing shear: Role of intercellular traction and cellular moments in collective cell migration. *Biochem Biophys Res Commun* **522**, 279–285 (2020).
36. Ng, M. R., Besser, A., Brugge, J. S. & Danuser, G. Mapping the dynamics of force transduction at cell–cell junctions of epithelial clusters. *Elife* **3**, (2014).
37. Gailit, J., Marchese, M. J., Kew, R. R. & Gruber, B. L. The differentiation and function of myofibroblasts is regulated by mast cell mediators. *J Invest Dermatol* **117**, 1113–9 (2001).
38. Berridge, M. J. Inositol trisphosphate and calcium signaling. *Nature* **361**, 315–325 (1993).
39. Munevar, S., Wang, Y. & Dembo, M. Regulation of mechanical interactions between fibroblasts and the substratum by stretch-activated Ca<sup>2+</sup> entry. *J Cell Sci* **117**, 85–92 (2004).
40. Bae, Y. S. *et al.* Activation of Phospholipase C- $\gamma$  by Phosphatidylinositol 3,4,5-Trisphosphate. *Journal of Biological Chemistry* **273**, 4465–4469 (1998).
41. Rhee, S. G. & Bae, Y. S. Regulation of Phosphoinositide-specific Phospholipase C Isozymes. *Journal of Biological Chemistry* **272**, 15045–15048 (1997).
42. Schrage, R. *et al.* The experimental power of FR900359 to study Gq-regulated biological processes. *Nat Commun* **6**, 10156 (2015).